Optical and Vibrational Properties of Toroidal Carbon Nanotubes

Florian Beuerle,[a] Carmen Herrmann,[a] Adam C. Whalley,[a] Cory Valente,[a] Alexander Gamburd,*[b] Mark A. Ratner,*[a] and J. Fraser Stoddart*[a]

Abstract: Toroidal carbon nanotubes (TCNTs), which have been evaluated for their potential applications in terahertz communication systems, provide a challenge of some magnitude from a purely scientific perspective. A design approach to TCNTs, as well as a classification scheme, is presented based on the definition of the six hollow sections that comprise the TCNT, slicing each of them to produce a (possibly creased) planar entity, and projecting that entity onto a graphene lattice. As a consequence of this folding approach, it is necessary to introduce five- and seven-membered rings as defect sites to allow the fusing together of the six segments into final symmetric TCNTs. This analysis permits the definition of a number of TCNT geometry families containing from 108 carbons up to much larger entities. Based on density functional theory (DFT) calculations, the energies of these structural candidates have been investigated and compared with [60]fullerene. The structures

Keywords: carbon · density functional calculations · nanotubes · optical and vibrational properties · toroid topology

with the larger tube diameters are computed to be more stable than C_{60}, whereas the smaller diameter ones are less stable, but may still be within synthetic reach. Computational studies reveal that, on account of the stiffness of the structures, the vibrational frequencies of characteristic low-frequency modes decrease more slowly with increasing ring diameter than do the lowest optical excitation energies. It was found that this particular trend is true for the "breathing mode" vibrations when the diameter of the tubes is small, but not for more flexible toroidal nanotubes with larger diameters.

Introduction

Shortly after their breaking upon the scientific landscapes, all-carbon nanostructures, be they fullerenes,[1] carbon nanotubes[2] or graphene,[3] began to revolutionize[4] the arenas of nanoscience, elemental semiconductor materials science, physics, and chemical physics. In all of these materials, sp^2-hybridized carbon atoms form stable trigonal bonds with the fourth π-orbital being singly occupied and thus conferring delocalized electronic character upon the different allotropes of carbon, which are defined by the connectivity of the trigonal bonds within their molecular structures. Despite the remarkable progress and achievements in research associated with this first generation of all-carbon materials, the search for sp^2-hybridized carbon structures with novel topol-

ogies is still proceeding apace, the objectives being both to attain fundamental understanding and to develop candidates for novel tailor-made materials with well-defined physical properties. In this context, toroidal carbon nanotubes (TCNTs) are of special interest on account of their unique geometries and topologies that are commensurate with potential properties differing significantly from those of existing nanostructures.

Since the first structure was proposed[5] in 1992, several different structural types of TCNTs have been both predicted theoretically and observed experimentally. Toroidal polyhexes can be created by connecting the ends of single-walled carbon nanotubes[6] (SWCNTs), and for bundles of linear carbon nanotubes, large toroidal structures with ring sizes larger than 100 nm have been observed experimentally.[7] Joining fullerenes with pentagonal and heptagonal rings into undulated ring systems or looped arrangements of Haeckelite tubules has also been proposed to give toroidal nanostructures.[8,9] For smaller ring sizes, the higher curvature induces a dramatic increase in the strain energy of TCNTs with all-hexagonal faces; yet, by incorporation of nonhexagonal defect sites, the strain energy can be reduced to a significant degree. Indeed, nonhexagonal defects in sp^2-hybridized carbon structures, inducing both positive and negative Gaussian curvature, have been observed experimentally.[10,11] In recent years, a variety of different structures have been proposed and studied theoretically.[12–14] Although experimental evidence for the structures has not yet been reported, quantum mechanical calculations predict[14,15]

[a] Dr. F. Beuerle, Dr. C. Herrmann, Dr. A. C. Whalley, Dr. C. Valente, Prof. Dr. M. A. Ratner, Prof. Dr. J. F. Stoddart
Department of Chemistry, Northwestern University
2145 Sheridan Road, Evanston, IL 60208-3113 (USA)
Fax: (+1) 847-491-1009
E-mail: stoddart@northwestern.edu
 ratner@chem.northwestern.edu

[b] Prof. Dr. A. Gamburd
Mathematics Department
University of California, Santa Cruz
1156 High Street, Santa Cruz, CA 95064-1077 (USA)
Fax: (+1) 831-459-3260
E-mail: agamburd@ucsc.edu

that they could exhibit larger or comparable cohesive energies than fullerenes and should therefore be thermodynamically stable.

On account of their quasi-zero-dimensional structures, these molecular systems have triggered a range of investigations concerning their electronic and magnetic properties.[16] Of special interest is the prediction of peculiar persistent currents[17] and exceptional magnetic responses[9,18] associated with these materials. Encapsulated systems containing fullerenes[19] or atomic metal loops[20] are described as potential gigahertz oscillators or composites with novel electromagnetic properties.

A further motivation for our investigation comes from pure mathematics, involving considerations related to expander graphs.[21,22] These are highly connected sparse graphs widely used in computer science. They have the property that, as the size of the graphs increases, the lowest eigenvalue of the Laplacian remains bounded away from zero. A separator theorem of Lipton and Tarjan[22] implies that, as the size of expander graphs increases, they necessarily become of higher genus. Since the normal mode frequencies of molecular structures are defined as those that are eigenvalues of the total vibration energy operator H_{vib}, which is the sum of the kinetic energy operator T and the potential energy operator V ($H_{vib} = T + V$), the relevant implication is that certain molecular structures of higher genus related to expander graphs should exhibit a lower limit for their vibrational frequencies. If the vibrational frequencies are all higher in energy than the lowest electronic transition, then these vibrations cannot broaden the spectral line. This lack of line broadening would give a huge Q factor for lines in this spectral region, namely the terahertz communication region. This phenomenon could lead to a fashioning of useful materials in a variety of fields such as terahertz communication systems. Construction of TCNTs is a first step in the exploration of these structures.

Spurred on by the prospect of useful applications for TCNTs, we are currently exploring synthetic strategies to obtain access to this exclusive and elusive class of all-carbon nanostructures. In concert with our synthetic efforts, we have carried out a structural appraisal of a series of different TCNTs with up to 500 carbon atoms from a theoretical standpoint, and compared their calculated vibrational and optical properties to their linear carbon nanotube analogues in order to assess how the special topology affects the vibrations as opposed to the electronic excitations of these exotic molecules.

Experimental Section

Computational methods: For the calculation of selected parts of the vibrational spectrum via the mode-tracking algorithm, Akira was used.[23] Step widths of 0.01 a.u. were employed for numerical energy derivatives with respect to nuclear displacements, unit matrices were used for preconditioning, and the convergence criteria for the mode-tracking calculations were set to 0.0005 a.u. for the maximum component of the residuum vector. As a representative example of a low-frequency mode, a

breathing mode was chosen as an initial guess. All calculations converged after one iteration. Unless otherwise mentioned, electronic structure calculations were performed with the quantum chemical program package Turbomole 5.71[24] using density functional theory and employing the BP86 functional[25] in combination with the resolution-of-the-identity ('RI') density fitting technique.[26] We used Ahlrichs' TZVP basis by Schaefer et al.[27] unless otherwise stated, which features a valence triple-zeta basis set with polarization functions on all atoms. Electronic excitation energies were calculated using time-dependent DFT (BP86/TZVP and SAOP[28]/TZP,[29] the latter using the Amsterdam Density Functional program package[29]). The full point-group symmetry of the molecular structures was exploited in all calculations.

Results and Discussion

Geometrical properties of toroidal carbon nanotubes: Recently, Chuang et al.[13,14] described an elegant classification scheme for TCNTs, which we decided to utilize for the construction of our model compounds. Topologically, a torus can be considered as an object having genus one and possessing one single hole. Since molecules are built up by discrete atoms, every suitable geometrical model for a molecular torus has to possess some degree of rotational symmetry other than C_∞. Therefore, a hollow prism with n-fold rotational symmetry can serve as a good model for TCNTs and, on account of its high symmetry, can be constructed (Figure 1 a) by employing a circular arrangement of n rotational unit cells. As shown by Chuang et al.,[14] cutting, unfolding, and projection onto a planar graphene surface give a two-dimensional representation (Figure 1 b) for the network of the tubular unit cell. Because of the hexagonal symmetry of graphene sheets, the parameter n_{rot}—indicating the number of repeated unit cells—should be close to six in order to avoid
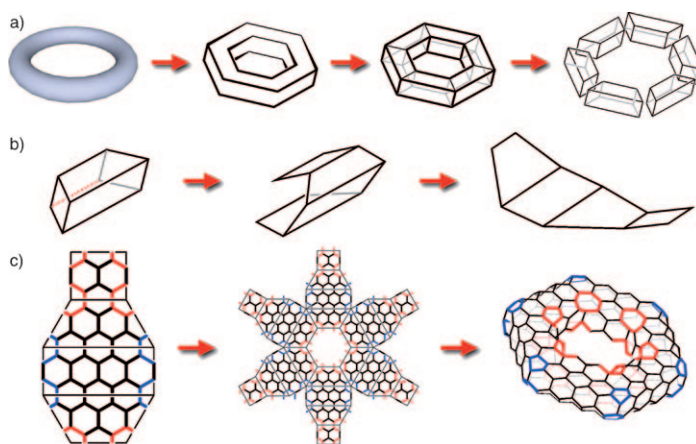

Figure 1. Toroidal carbon nanotubes can be considered as hollow prisms with rotational symmetry: a) Construction by a repeating ring-like arrangement of rotational unit cells. b) Two-dimensional networks of a rotational unit cell are obtained by cutting and unfolding the tubular unit cell. c) Projection of the 2D network onto a graphene sheet and subsequent folding leads to a 3D model of a TCNT. This geometrical construction introduces an equal number of seven-membered rings (red) on the inside of the toroid and five-membered rings (blue) on the outside of the toroid, minimizing the strain energy in this curved structure compared to bent all-hexagon carbon nanotubes.

unnecessary strain energy in the final toroidal structure. For $n_{rot} = 6$, the unit cell networks can be arranged (Figure 1c) on a graphene sheet without any distortion, a situation which would not be possible for any other value of n_{rot}. In addition, quantum chemical calculations on various TCNTs with different n_{rot} values have suggested[14] that the most stable structures are indeed obtained for $n_{rot} = 6$ or, in a few cases when $n_{rot} = 5$ or 7. In all other cases, the optimized structures are significantly higher in energy. In the discussion which follows, we will focus on toroidal systems with $n_{rot} = 6$.

Cutting and folding of the two-dimensional network leads (Figure 1c) to the formation of a polygonal TCNT with hexagonal symmetry. The small and large rectangles of the rotational unit cells correspond to the inner and outer rims of the toroidal structures, respectively, whereas the two trapezoidal portions form the upper and lower rings of the torus. As a result of the cutting and folding processes, the hexagons on the vertices of the three-dimensional torus are reconfigured (Figure 1) to pentagons and heptagons. Since all closed polygonal surfaces must satisfy Euler's formula,[30] $\chi = V - E + F$, in which V, E, and F are the numbers of vertices, edges, and faces of the polygon, respectively, and χ is the Euler characteristic of the surface ($\chi = 0$ for a genus-one surface), the algebraic transformations (see Supporting Information) give $N_5 = N_7$ (N_x denotes the number of x-membered rings), indicating that every toroidal network of hexagons, pentagons, and heptagons must have equal numbers of five- and seven-membered rings with no constraint on N_6. Thereby, all heptagons (red) are arranged in the inner rim, whereas all pentagons (blue) are located on the outer rim (Figure 1c). The introduction of pentagons and heptagons into graphene sheets results in positive and negative Gaussian curvature, respectively, and therefore greatly reduces the strain energy of the curved TCNT in comparison to bent, defect-free nanotubes. For carbon nanotubes possessing the so-called 5–7 pair couple defects, bent structures have been observed experimentally.[11]

Each particular rotational unit cell is described by a set of two parameters introduced by Chuang et al.[14] Firstly, the chirality of the resulting TCNT is defined by the concomitant alignment of the unfolded unit cell with respect to the graphene lattice vectors. Following the usual notation[31] for chiral SWCNTs, the chirality of the TCNT is introduced by aligning the base vector of the unit cell along the chirality vector (n_1, n_2) with $0 < n_1/n_2 < 1$ and no common divisor for n_1 and n_2. In common with linear SWCNTs, there are only two different achiral structures—with chiral vectors (1,0) and (1,1)—whereas all other possible chiral vectors lead (Figure 2a) to chiral structures. For reasons of simplicity, only achiral TCNTs will be discussed here, on the understanding that all our considerations can also be applied to their chiral analogues. For the chiral vector (1,0), the hexagons around the outer and inner rim are arranged in a zigzag alignment, whereas for (1,1), the six-membered rings exhibit an armchair configuration; that is, these two structural types correspond to zigzag and armchair SWCNTs in the
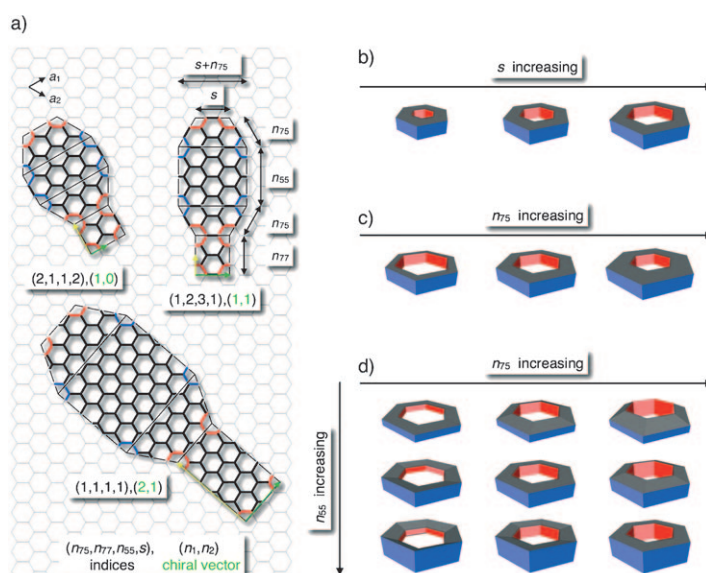

Figure 2. a) A description of selected rotational unit cells on graphene sheets with reference to two sets of parameters. The chiral vector (green) indicates the orientation of the base vector in relation to the lattice vectors a_1 and a_2. By analogy with linear nanotubes, chiral vectors (1,0) and (1,1) give achiral TCNTs, whereas all other chiral vectors lead to chiral TCNTs. The four parameters s, n_{75}, n_{77} and n_{55}, determine the size and geometrical shape of the resulting TCNT. b) Increasing s leads to larger ring sizes with a constant tube diameter. c) Increasing n_{75} leads to larger tube diameters with a constant toroidal circumference. d) Increasing n_{77} and n_{55} leads to structures with higher inner (n_{77}) and outer (n_{55}) rings. For large values, $n_{55} = n_{77}$, TCNTs converge to double-walled CNTs.

linear case. The second set of parameters is defined by the four numbers n_{75}, n_{77}, n_{55}, and s. The value of n_{75} defines the distance from the pentagons to heptagons, whereas the height of the inner and outer rim is set by n_{77} and n_{55}, respectively. Finally, parameter s determines the width of the unit cell.

For a geometrical interpretation of these indices, three series of different TCNT models, each representing a systematic change of one or two parameters, are depicted in Figure 2b–d. Figure 2b shows different TCNTs with increasing s and constant n_{75}, n_{77}, and n_{55}. This modification leads to an increased ring size, but does not affect the tube diameter of the torus. Here, and in the following discussion, "ring diameter" or "size" refers to the larger ring (torus), which may be formed by the bending of a nanotube. Increasing the ring size can be rationalized by inserting linear CNT fragments between the bends containing the non-hexagon defects. For the large s limit, these structures become quite similar to large all-hexagon TCNTs without any defect sites. By changing only the parameter n_{75} (Figure 2c), the ratio between the diameters of the inner and outer rim can be modified, resulting in a change of the tube diameter, a situation which corresponds to a change of the roll-up vector for linear carbon nanotubes. The effects of changing the values of both n_{77} and n_{55} are illustrated in Figure 2d. Increasing n_{77} and n_{55} values lead to an increase in the height of the inner and outer rims, respectively. Therefore, the diagonal struc-

tures with $n_{77} = n_{55}$ show a series of TCNTs with increasing height of the toroid with no significant change in the circumference. The tube diameter becomes more distorted from a perfect circle towards an ellipse, and in the large n limit case, these structures converge to double-walled carbon nanotubes.[32]

For this parent type of TCNT, both five- and seven-membered rings are arranged in line with each other on one cross-section through the torus, resulting in a hollow prism shape with D_{6h} symmetry (D_{nh} for $n_{rot} = n$) as shown in Figure 3 (structure-type **I**). However, there are two kinds of isomerization, both of which retain the high rotational symmetry of the toroidal structures but change the relative positions of the defect sites with respect to each other. On the one hand, concerted Stone–Wales transformations[33] of either pentagon or heptagon pairs change their relative arrangement to a staggered configuration (structure-type **II** in Figure 3a). On the other hand, appropriate horizontal shifting of the upper rim relative to the lower rim of the torus results in a D_{6d} (D_{nd} for $n_{rot} = n$) symmetrical hollow antiprism (structure-type **III** in Figure 3a). In the case of these structures, both the pentagons on the outer rim and the heptagons on the inner rim are now arranged in an alternate fashion in contrast to the aligned arrangement in the structure-type **I**. A combination of both Stone–Wales transformations and horizontal shifting gives the structure-type **IV**. For these structures, the defect sites are in an all-staggered arrangement on a single cross-section through the toroid. We can recall that there are two different achiral TCNT structures with the chiral vectors (1,0) and (1,1) possessing struc-

tural-type **I**. Therefore, each parent structure can be transformed to three different structures of types **II–IV**, giving a total of eight different families of highly symmetrical TCNTs **A–H**. Figure 3b shows both two-dimensional representations of the rotational unit cells and MMFF94-minimized[34] (Merck molecular force field (MMFF94) implemented in the molecular modeling software SPARTAN '06[35]) 3D structures of one example of each family possessing 288 (**A**, **C**, **D**, **F**, **G**, and **H**) or 300 (**B** and **E**) carbon atoms. Note that the concerted Stone–Wales transformations of pentagon or heptagon pairs change the arrangement of hexagons in the outer or inner rim from zigzag to armchair or vice versa, for example, by going from **C** to **G** (Stone–Wales transformation of pairs of heptagons, in which the inner rim is changed from zigzag to armchair) or **H** (Stone–Wales transformation of pairs of pentagons, in which the outer rim is transformed from zigzag to armchair). These observations result in the formation of TCNTs with a different orientation of the hexagons in the inner and outer rims, for example, **E** with zigzag in the outer and armchair in the inner rim or **H** with armchair in the outer and zigzag in the inner rim. Especially for structures with large n_{77} and n_{55} values that reach the limit leading to double-walled linear carbon nanotubes, this approach might be particularly important for potential applications, since some effects and properties of both armchair and zigzag carbon nanotubes can be combined in one molecule in this case. For D_{6d} symmetrical TCNTs, on account of complicated mathematical issues,[14] the Stone–Wales transformations described here do not correspond to isomerization processes and therefore the
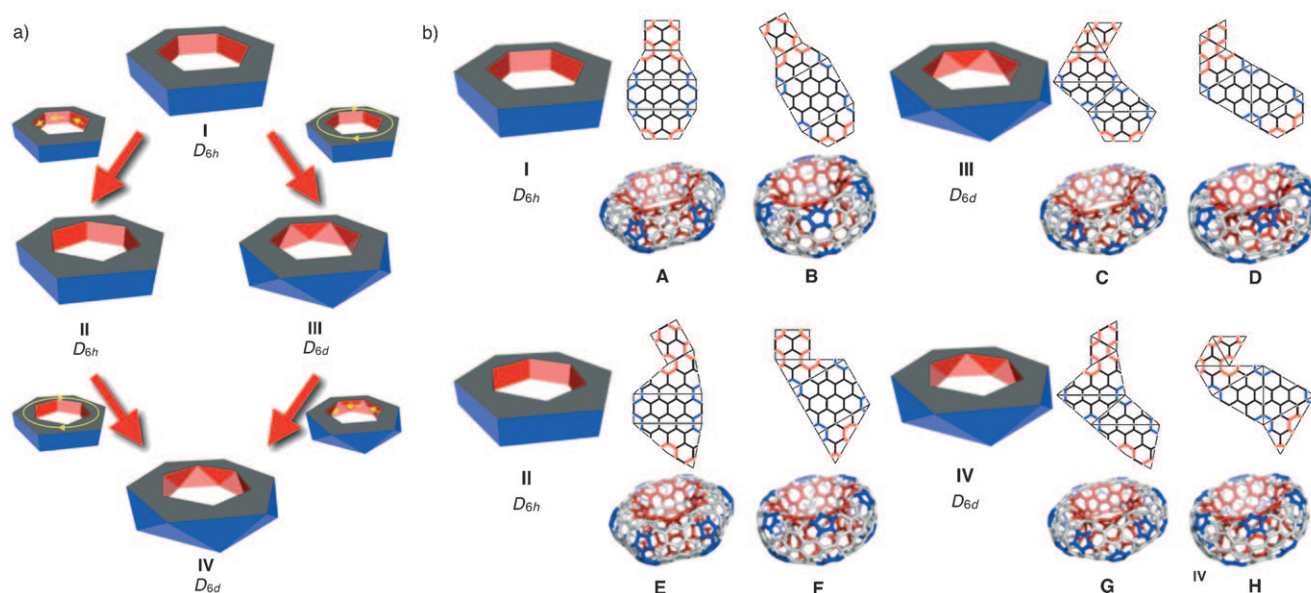

Figure 3. a) Three other types of high-symmetry TCNTs can be constructed by geometrical transformations of the parent-type **I** with D_{nh} symmetry (with $n_{rot} = 6$ in all cases in this work, the point group is D_{6h}). Concerted Stone–Wales transformations of pentagon or heptagon pairs give structure-type **II**, in which the inner rim is shifted with respect to the outer rim. Horizontal shifting of the upper rim of a hollow prism results in the formation of hollow antiprisms of structure-type **III** with D_{nd} symmetry. A combination of both geometrical transformations leads to structure type-**IV**. b) Each structure type has two achiral representatives with chiral vectors (1,0) (**A**, **C**, **F**, and **H**) and (1,1) (**B**, **D**, **E**, and **G**). Structure-types **A–H** represent the eight different types of high-symmetry TCNT isomers only differing in the relative arrangement of both five- and seven-membered defect sites. For each structure type, 2D unit cells and geometry-optimized molecular structures for TCNTs with 288 (**A**, **C**, **D**, **F**, **G**, and **H**) or 300 (**B** and **E**) carbon atoms are shown.

number of carbon atoms is essentially changed by going from **A** to **E** or **B** to **F**.

Structures under investigation: To test our hypothesis that the vibrational frequencies decrease more slowly with the increasing ring size compared to the lowest optical transitions for these unique carbon nanostructures, we constructed two series of TCNTs with defined structural changes and performed DFT quantum chemical calculations. So far, our synthetic efforts have been mainly focused on TCNTs of structure-type **A** (Figure 3b), since we believe this class of compounds should be the easiest to access synthetically. In all the calculations, therefore, we focused on TCNTs of this type. For comparison, and to ascertain if the topological genus and mode of connectivity of the molecular structures play any role in determining selected optical and vibrational properties, we also performed calculations on linear analogues, for example, linear carbon nanotubes.

Starting with the smallest possible derivative, that is, for $n_{rot} = 6$, we obtained (Figure 4a) the **TCNT-1** (C_{108}) with ($n_{rot} = 6$, (1,1,1,1),(1,0)). For a linear analogue, we constructed the single-walled carbon nanotube, **SWCNT-1** ($C_{108}H_{12}$), with the roll-up vector (3,3) and the translation vector (9,0), exhibiting the same tube diameter with a linear, defect-free all-hexagon structure. Furthermore, we have investigated the effects of changing the structural parameter n_{75} by constructing **TCNT-2** (C_{192}, Figure 4a) with ($n_{rot} = 6$, (2,1,1,1), (1,0)) and the analogous linear carbon nanotube, **SWCNT-2** ($C_{196}H_{16}$), with a roll-up vector of (4,4). Additionally (Figure 4b), we changed only the parameter s and created the
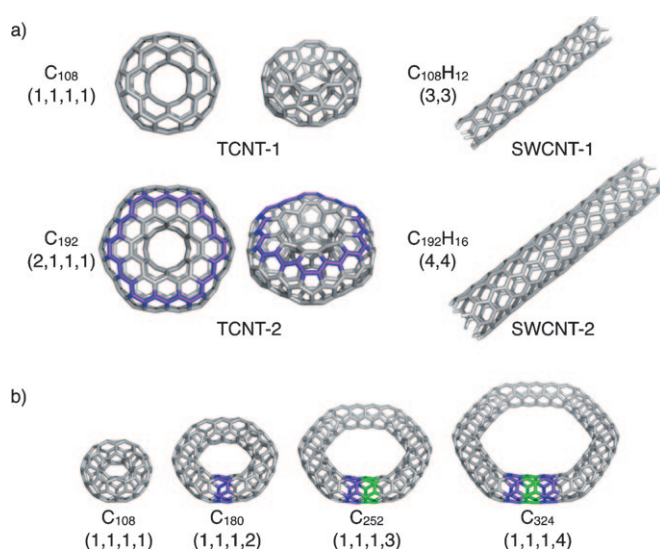
TCNT-1 series C_{108}, C_{180}, C_{252}, and C_{324} ($n_{rot} = 6$, (1,1,1,s), (1,0); $s = 1$–4). This structural change can be rationalized by adding subsequently (3,3) nanotube fragments in between two sets of defect sites into the toroidal structure, as shown by the violet and green atoms in Figure 4b. This exercise leads to overall elongation without changing the tube diameter in the linear case. Structural models and atomic coordinates for all calculated molecules are provided in the Supporting Information.

Computational approach: To investigate the electronic properties of TCNTs and compare them to their linear analogues to evaluate their potential as materials for novel technologies, we calculated selected optical and vibrational properties for the four molecular series **TCNT-1**, **SWCNT-1**, **TCNT-2**, and **SWCNT-2** as shown in Figure 4. Our focus is on whether the frequencies of the breathing modes decrease more slowly with the increasing ring size of the TCNTs compared with the lowest symmetry-allowed electronic transitions and whether the frequencies of the breathing modes decrease more slowly for the toroidal systems than for their linear counterparts.

We optimized the geometry of structural representatives of all the series, **TCNT-1**, **TCNT-2**, **SWCNT-1**, and **SWCNT-2**, using DFT with a BP86 functional[25] and a basis set of triple-zeta split-valence quality with polarization functions on all atoms (TZVP[27]). This combination tends to give accurate vibrational frequencies within the harmonic approximation.[36] Optical excitation energies were obtained from single-point calculations on the BP86/TZVP optimized structures, using statistical average of orbital potentials[28] (SAOP) in combination with a basis set[29] of approximately the same quality (TZP).

Thermodynamic stability: To assess the thermodynamic stability of the TCNTs, we used the most abundant and stable fullerene, C_{60}, as a reference compound. To compare molecular systems of different sizes, we calculated the total energies, that is, electronic energies plus the internuclear repulsion, relative to the number of carbon atoms in comparison to C_{60}. While these energies per carbon atom are straightforward to compute for carbon-only compounds such as TCNTs, it is unclear how to partition the energy between carbon and hydrogen atoms in our hydrogen-capped SWCNTs. Therefore, these data have not been included in the comparison. Nevertheless, this does not exclude the possibility that, from a synthetic point of view, the SWNCTs may be even more stable than the TCNTs. Positive energies indicate that the structures are less stable, and negative energies that they are more stable than C_{60}. Absolute values of all energies are given in the Supporting Information. The members of the **TCNT-2** series are significantly more stable than those of the **TCNT-1** structures (Figure 5a), since the smaller tube diameter for **TCNT-1** induces more strain energy. Increasing the parameter s in each series leads to more stable structures and, in the very large limit, these series are expected to reach the energy per atom of the cor-
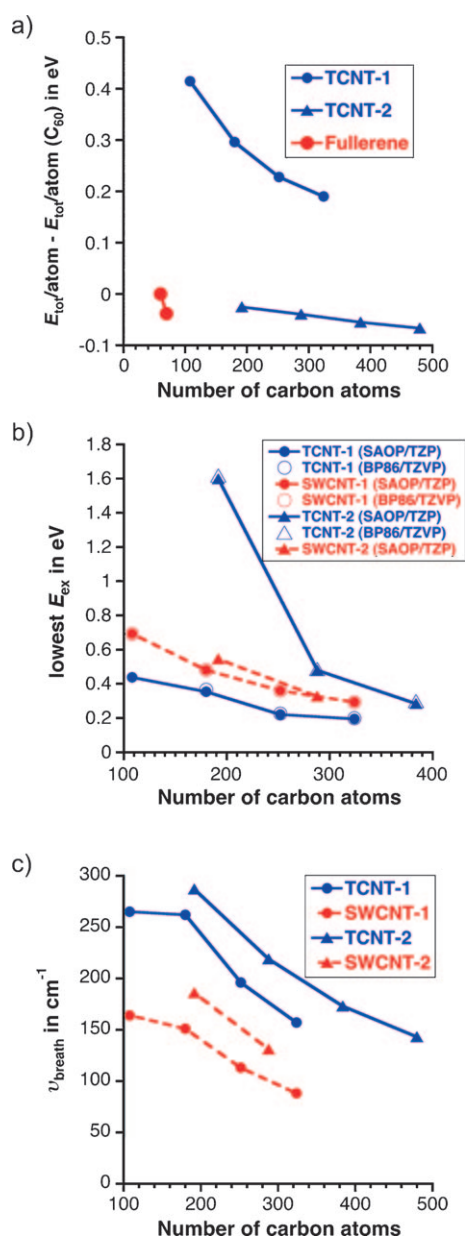

Figure 4. a) Two types of TCNTs, **TCNT-1** ($n_{rot} = 6$, (1,1,1,1),(1,0)) and **TCNT-2** ($n_{rot} = 6$, (2,1,1,1),(1,0)) with increasing parameter n_{75}. The increase in n_{75} can be rationalized by adding additional rings of carbon atoms in the upper and lower rim of the TCNT (violet atoms). For the linear analogues **SWNT-1** and **SWNT-2**, increasing the roll-up vector (x,x) by one unit is consistent with increasing n_{75} by one unit. b) **TCNT-1** series ($n_{rot} = 6$, (1,1,1,s),(1,0)) with increasing parameter s. The increase in s can be rationalized by adding additional fragments of linear nanotubes in between the defect sites (violet and green atoms).

Figure 5. a) Total energy per atom for **TCNT-1** and **TCNT-2** series in relation to the energy per atom of C_{60}. b) Lowest excitation energies E_{ex} calculated at the TDDFT level (SAOP/TZP and BP86/TZVP) in relation to the number of carbon atoms for **TCNT-1**, **TCNT-2**, **SWCNT-1**, and **SWCNT-2**. c) Frequencies for the radial breathing modes for **TCNT-1**, **TCNT-2**, **SWCNT-1**, and **SWCNT-2** determined by the mode-tracking algorithm.

responding infinite linear SWCNT with the appropriate roll-up vector. Compared to the reference fullerene, all derivatives of **TCNT-2** exhibit lower total energies per atom than the known molecule C_{60}, making these structures very promising candidates for synthesis. These observations encourage us to pursue our synthetic efforts towards **TCNT-2** derivatives. For the **TCNT-1** series, the energies per atom are slightly higher than for C_{60} fullerenes.

Optical properties: For investigations on the optical properties, we calculated the lowest symmetry-allowed electronic excitation energies for all the series **TCNT-1**, **TCNT-2**, **SWCNT-1**, and **SWCNT-2** by employing time-dependent DFT (TDDFT). Two different combinations of functionals and basis sets, SAOP/TZP and BP86/TZVP, were used in order to determine the reliability of these calculations. Since the two functionals showed very good agreement for all structures, all results should be accurate within the limitations of TDDFT, and no major artifacts resulting from the functional should be observed. A linear plot (Figure 5b) of the first excitation energies against the number of carbon atoms reveals that for the linear series, **SWCNT-1** and **SWCNT-2**, the effect of changing the curvature by going from **SWCNT-1** to **SWCNT-2** is small, and the lowest allowed excitation energy depends primarily on the overall size of the π-system, namely, the number of carbon atoms. From our limited data set, it can be estimated that this dependence is approximately linear. However, for larger systems other effects, such as the tube helicity, have to be taken into account, just as some types of SWCNTs, depending on their chirality, are metallic or semiconducting.[37] For the toroidal systems, the introduction of additional strain as a result of the ring closure and the presence of pentagon and heptagon defect sites causes additional effects on the electronic properties of these systems. Especially for the small derivatives of **TCNT-2**, the combination of a bigger tube diameter and a small ring size might result in stronger effects due to the bending into a torus, a higher distortion of the π system and therefore higher excitation energies. With increasing parameter *s*, these effects become smaller and it might be anticipated that for larger *s* values, excitation energies for both toroidal and linear analogues are mainly determined by the number of carbon atoms, that is, by the size of the π system. While for the **SWCNT-1/TCNT-1** series, the excitations of the linear species are below those for the toroidal ones, the opposite is true for the series with the larger tube diameter (**SWCNT-2/TCNT-2**). On account of computational limits, we were restricted to the analysis of molecular structures with less than 500 atoms, and in this range, the lowest allowed excitation energies still depend subtly on the individual structural parameters of the molecules.

Vibrational properties: For molecular systems of this size (up to 500 atoms), full vibrational calculations that are quantitatively accurate are very close to, or perhaps beyond the limit of, current computational resources. However, it is possible to calculate certain low-energy vibrations, for example, breathing modes, selectively with very little computational effort using algorithms such as mode tracking.[23] In this approach, specific vibrations can be chosen by an initial guess and then refined in a subspace-iteration approach, yielding exact normal modes within the harmonic approximation, that is, vibrational motion is described as a set of decoupled harmonic oscillators. Although this approximation typically works well for high-frequency modes, for lower frequencies, the potential energy as a function of elon-

gation along the normal mode may deviate significantly from being quadratic. Therefore, we do not expect a reliable description of the nature and frequency of the lowest-lying mode within our model, even if the full vibrational spectrum could be calculated. Thus, we decided instead to focus on one characteristic type of vibration that is typically expected to have a low vibrational frequency. We chose breathing modes for both the TCNT and SWCNT series as a representative example of one of the lowest vibrational modes. Graphical representations for the calculated breathing modes for both **TCNT-1** and **SWCNT-1** are given in Figure 6. The calculated frequencies ν_{breath} are plotted (Figure 5c) against the number of carbon atoms for all structures. The breathing modes for the more rigid toroidal systems are higher in energy than for their linear analogues.
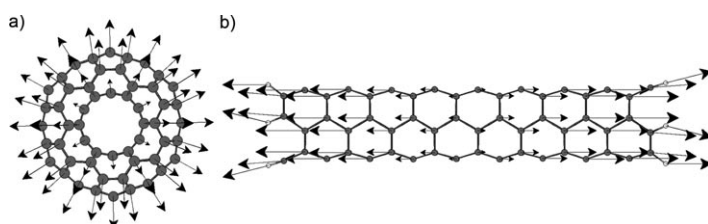

Figure 6. Graphical representation of the calculated breathing mode for a) **TCNT-1** ((1,1,1,1),(1,0), C_{108}) as a representative of the TCNT series and b) **SWCNT-1** ((3,3),(9,0), $C_{108}H_{12}$) as a representative of the SWCNT series.

This observation may be attributed both to the different qualitative nature of the breathing modes in the two systems (Figure 6) and the stiffer structure of the toroidal systems. This situation may be contrasted with the toroidal systems that have lower optical excitation energies than the linear ones for the structures with the smaller tube diameter. Increasing tube diameter results in higher vibrational frequencies for both the linear and toroidal systems. On the other hand, an increase in the ring size or tube length leads to lower energies for the breathing modes. In this context, there might be a first hint within the range of our limited dataset—with fewer than 500 atoms—that selected low-lying vibrational frequencies for the toroidal systems decrease more slowly with increasing number of carbon atoms than for their linear counterparts. In order to make a more definite statement, calculations on larger structures and analyses of the full vibrational spectrum would have to be performed, an exercise that is beyond the scope of this work.

Conclusion

We have identified a series of eight different families (**A–H**) of TCNTs varying in the relative arrangement of both pentagons and heptagons as defect sites, in addition to regular hexagons. For each family, sets of five parameters control the overall size and shape of the toroidal molecular structure. Following this scheme, we can easily cover every possi-

ble high-symmetry TCNT structure built up by a closed network of five-, six-, and seven-membered rings.

Additionally, we have investigated the dependence of the "breathing mode" vibrational frequencies and the lowest symmetry-allowed electronic excitations for a series of toroidal carbon nanotubes that vary in ring and tube diameter, and have compared them to their linear carbon nanotube counterparts. We find that for structures with smaller tube diameter, the vibrational wave number of the breathing mode is always higher for the toroidal species than for the linear one, whereas the lowest allowed electronic excitation is higher for the linear species than for the toroidal one. As far as the vibrational properties are concerned, the same is true for the systems with larger tube diameter, but for the electronic excitations, the relation is inverted. This behavior suggests that the topology of the toroidal structures may put stronger constraints on the lower bound for vibrational frequencies than it does for electronic ones, provided the tube diameter is small. For the systems under investigation here, both electronic and vibrational excitation energies decrease with increasing ring parameters.

The thermodynamic stability of toroidal structures with a large tube diameter is predicted to be larger than for fullerenes, which suggests that they may be synthetically accessible. Research along these lines is currently underway in our laboratories.

[1] H. W. Kroto, J. R. Heath, S. C. O'Brien, R. F. Curl, R. E. Smalley, *Nature* **1985**, *318*, 162–163.

[2] S. Iijima, *Nature* **1991**, *354*, 56–58.

[3] K. S. Novoselov, A. K. Geim, S. V. Morozov, D. Jiang, Y. Zhang, S. V. Dubonos, I. V. Grigorieva, A. A. Firsov, *Science* **2004**, *306*, 666–669.

[4] a) A. Hirsch, M. Brettreich, *Fullerenes—Chemistry and Reactions*, Wiley-VCH, Weinheim, **2005**; b) A. K. Geim, K. S. Novoselov, *Nat. Mater.* **2007**, *6*, 183–191; c) Y. Ando, *J. Nanosci. Nanotechnol.* **2010**, *10*, 3726–3738.

[5] B. I. Dunlap, *Phys. Rev. B* **1992**, *46*, 1933–1936.

[6] a) E. C. Kirby, R. B. Mallion, P. Pollak, *J. Chem. Soc. Faraday Trans.* **1993**, *89*, 1945–1953; b) V. Meunier, P. Lambin, A. A. Lucas, *Phys. Rev. B* **1998**, *57*, 14886–14890; c) L. Liu, G. Y. Guo, C. S. Jayanthi, S. Y. Wu, *Phys. Rev. Lett.* **2002**, *88*, 217206.

[7] a) J. Liu, H. Dai, J. H. Hafner, D. T. Colbert, R. E. Smalley, S. J. Tans, C. Dekker, *Nature* **1997**, *385*, 780–781; b) M. Ahlskog, E. Seynaeve, R. J. M. Vullers, C. Van Haesendonck, A. Fonseca, K. Hernadi, J. B. Nagy, *Chem. Phys. Lett.* **1999**, *300*, 202–206; c) R. Martel, H. R. Shea, P. Avouris, *Nature* **1999**, *398*, 299; d) R. Martel, H. R. Shea, P. Avouris, *J. Phys. Chem. B* **1999**, *103*, 7551–7556; e) M.

Sano, A. Kamino, J. Okamura, S. Shinkai, *Science* **2001**, *293*, 1299–1301; f) Y. Wang, D. Maspoch, S. Zou, G. C. Schatz, R. E. Smalley, C. A. Mirkin, *Proc. Natl. Acad. Sci. USA* **2006**, *103*, 2026–2031.

[8] H. Terrones, M. Terrones, E. Hernandez, N. Grobert, J. C. Charlier, P. M. Ajayan, *Phys. Rev. Lett.* **2000**, *84*, 1716–1719.

[9] J. A. Rodríguez-Manzo, F. Lopez-Urias, M. Terrones, H. Terrones, *Nano Lett.* **2004**, *4*, 2179–2183.

[10] a) S. Iijima, T. Ichihashi, Y. Ando, *Nature* **1992**, *356*, 776–778; b) R. Tamura, M. Tsukada, *Phys. Rev. B* **1994**, *49*, 7697–7708; c) A. Krishnan, E. Dujardin, M. M. J. Treacy, J. Hugdahl, S. Lynum, T. W. Ebbesen, *Nature* **1997**, *388*, 451–454; d) A. Hashimoto, K. Suenaga, A. Gloter, K. Urita, S. Iijima, *Nature* **2004**, *430*, 870–873.

[11] K. Suenaga, H. Wakabayashi, M. Koshino, Y. Sato, K. Urita, S. Iijima, *Nat. Nanotechnol.* **2007**, *2*, 358–360.

[12] a) S. Itoh, S. Ihara, *Phys. Rev. B* **1993**, *48*, 8323–8328; b) S. Ihara, S. Itoh, J. Kitakami, *Phys. Rev. B* **1993**, *47*, 12908–12911; c) S. Itoh, S. Ihara, J. Kitakami, *Phys. Rev. B* **1993**, *47*, 1703–1704; d) S. Itoh, S. Ihara, *Phys. Rev. B* **1994**, *49*, 13970–13974; e) J. E. Avron, J. Berger, *Phys. Rev. A* **1995**, *51*, 1146–1149; f) J. Berger, J. E. Avron, *J. Chem. Soc. Faraday Trans.* **1995**, *91*, 4037–4045; g) R. Setton, N. Setton, *Carbon* **1997**, *35*, 497–505.

[13] C. Chuang, Y.-C. Fan, B.-Y. Jin, *J. Chem. Inf. Model.* **2009**, *49*, 1679–1686.

[14] C. Chuang, Y.-C. Fan, B.-Y. Jin, *J. Chem. Inf. Model.* **2009**, *49*, 361–368.

[15] a) B. Borstnik, D. Lukman, *Chem. Phys. Lett.* **1994**, *228*, 312–316; b) D. H. Oh, J. M. Park, K. S. Kim, *Phys. Rev. B* **2000**, *62*, 1600–1603; c) C. Chuang, B.-Y. Jin, *J. Mol. Graphics Modell.* **2009**, *28*, 220–225.

[16] a) K. Sasaki, *Phys. Rev. B* **2002**, *65*, 155429; b) C. G. Rocha, M. Pacheco, Z. Barticevic, A. Latge, *Phys. Rev. B* **2004**, *70*, 233402.

[17] a) M. F. Lin, D. S. Chuu, *Phys. Rev. B* **1998**, *57*, 6731–6737; b) S. Latil, S. Roche, A. Rubio, *Phys. Rev. B* **2003**, *67*, 165420; c) R. B. Chen, B. J. Lu, C. C. Tsai, C. P. Chang, F. L. Shyu, M. F. Lin, *Carbon* **2004**, *42*, 2873–2878; d) C. C. Tsai, F. L. Shyu, C. W. Chiu, C. P. Chang, R. B. Chen, M. F. Lin, *Phys. Rev. B* **2004**, *70*, 075411; e) N. Xu, J. W. Ding, H. B. Chen, M. M. Ma, *Eur. Phys. J. B* **2009**, *67*, 71–75.

[18] a) M.-F. Lin, *J. Phys. Chem. Soc. Jpn.* **1998**, *67*, 1094–1097; b) L. Liu, G. Y. Guo, C. S. Jayanthi, S. Y. Wu, *Phys. Rev. Lett.* **2002**, *88*, 217206; c) F.-L. Shyu, *Phys. Rev. B* **2005**, *72*, 045424; d) R. Tamura, M. Ikuta, T. Hirahara, M. Tsukada, *Phys. Rev. B* **2005**, *71*, 045418.

[19] T. A. Hilder, J. M. Hill, *J. Appl. Phys.* **2007**, *101*, 064319.

[20] M. T. Lusk, N. Hamm, *Phys. Rev. B* **2007**, *76*, 125422.

[21] a) N. Alon, P. Seymour, R. Thomas, *J. Am. Math. Soc.* **1990**, *3*, 801–808; b) J. Bourgain, A. Gamburd, *Ann. Math.* **2008**, *167*, 625–642; c) P. Sarnak, *Not. Am. Math. Soc.* **2004**, *51*, 762–763.

[22] R. J. Lipton, R. E. Tarjan, *SIAM J. Appl. Math.* **1979**, 36.

[23] a) M. Reiher, J. Neugebauer, *J. Chem. Phys.* **2003**, *118*, 1634–1641; b) C. Herrmann, J. Neugebauer, M. Reiher, *New J. Chem.* **2007**, *31*, 818–831; c) AKIRA—the Mode-Tracking program for the purpose-driven calculation of pre-selected molecular vibrations, J. Neugebauer, C. Herrmann, K. Kiewisch, S. Luber, S. Schenk, M. Reiher, http://www.reiher.ethz.ch/software/akira.

[24] R. Ahlrichs, http://www.cosmologic.de/turbomole.html.

[25] a) J. P. Perdew, *Phys. Rev. B* **1986**, *33*, 8822–8824; b) A. D. Becke, *Phys. Rev. A* **1988**, *38*, 3098–3100.

[26] a) E. J. Baerends, D. E. Ellis, P. Ros, *Chem. Phys.* **1973**, *2*, 41–51; b) B. I. Dunlap, J. W. D. Connolly, J. R. Sabin, *J. Chem. Phys.* **1979**, *71*, 3396–3402; c) ftp://ftp.chemie.uni-karlsruhe.de/pub/jbasen.

[27] ftp://ftp.chemie.uni-karlsruhe.de/pub/basen.

[28] P. R. T. Schipper, O. V. Gritsenko, S. J. A. van Gisbergen, E. J. Baerends, *J. Chem. Phys.* **2000**, *112*, 1344–1352.

[29] a) G. te Velde, F. M. Bickelhaupt, S. J. A. van Gisbergen, C. Fonseca Guerra, E. J. Baerends, J. G. Snijders, T. Ziegler, *J. Comput. Chem.* **2001**, *22*, 931–967; b) C. Fonseca Guerra, J. G. Snijders, G. te Velde, E. J. Baerends, *Theor. Chem. Acc.* **1998**, *99*, 391–403; c) ADF2009.01, SCM, Theoretical Chemistry, Vrije Universiteit, Amsterdam (The Netherlands), http://www.scm.com.

[30] H. W. Kroto, A. W. Allaf, S. P. Balm, *Chem. Rev.* **1991**, *91*, 1213–1235.

[31] N. Hamada, S. Sawada, A. Oshiyama, *Phys. Rev. Lett.* **1992**, *68*, 1579–1581.

[32] A. Sarkar, H. W. Kroto, M. Endo, *Carbon* **1995**, *33*, 51–55.

[33] A. J. Stone, D. J. Wales, *Chem. Phys. Lett.* **1986**, *128*, 501–503.

[34] T. A. Halgren, *J. Comput. Chem.* **1996**, *17*, 490–519.

[35] SPARTAN 06, Version 1.1.1, http://www.wavefun.com.

[36] J. Neugebauer, B. A. Hess, *J. Chem. Phys.* **2003**, *118*, 7215–7225.

[37] J. W. G. Wilder, L. C. Venema, A. G. Rinzler, R. E. Smalley, C. Dekker, *Nature* **1998**, *391*, 59–62.